OPEN

# Mapping Gadolinium-based Contrast Agent Residues in the Rat Kidney

*Luis Hummel, MSc, Janina Boyken, PhD, Thomas Gladytz, PhD, Axel Treu, PhD, Ehsan Tasbihi, PhD, Thoralf Niendorf, PhD, Hubertus Pietsch, VMD, and Erdmann Seeliger, MD*

**Objectives:** Gadolinium-based contrast agents (GBCAs) are routinely used to enhance magnetic resonance (MR) imaging. In recent years, GBCA residues were detected in multiple organs, with the kidney as the primary organ of excretion showing the highest concentrations. This study aimed to map the intricate spatial distribution of GBCA residues in rat kidneys at an early and a late time point.

**Materials and Methods:** Rats received one of 6 marketed GBCAs [3 macrocyclic, 3 linear; cumulative dose 4.8 mmol gadolinium (Gd)/kg] or saline and were sacrificed at day 5 or week 14 post administration (n = 5 per GBCA and time point). In whole renal tissue slices, the distribution of elemental Gd was determined by laser ablation–inductively coupled plasma–mass spectrometry and the distribution of intact GBCA chelates by matrix-assisted laser desorption ionization–mass spectrometry imaging. In *ex vivo* kidneys, MR relaxometry was used to assess MR-detectable GBCA residues.

**Results:** At day 5, Gd was predominantly localized in the renal cortex across all GBCAs, with 10- to 100-fold lower medullary levels. Distribution patterns corresponded well with those of exemplary intact GBCA chelates. At week 14, Gd levels had decreased by 1 to 2 orders of magnitude. Distribution patterns from linear GBCAs showed Gd remaining predominantly in the cortex, while Gd from macrocyclic GBCAs was similar in cortex and medulla. Several GBCAs exhibited a prominent Gd presence at the transition zone between outer and inner medulla. Intact chelate was only detectable for the exemplary macrocyclic GBCA, with a spatial distribution pattern matching that of elemental Gd. MR relaxometry detected GBCA residues within *ex vivo* kidneys but also in the surrounding water-based fixative. This indicated the presence and washout of intact GBCAs, which was greater for macrocyclic versus linear GBCAs.

**Conclusions:** This study provides the first comprehensive spatially resolved characterization of renal GBCA residues at an early and a late time point. GBCA residues exhibited specific intrarenal distribution patterns and distinct changes in these patterns over the course of their elimination. Our findings of specific retention patterns suggest that renal microanatomy and local physicochemical conditions play critical roles in GBCA retention. These insights provide a foundation for future investigations into retention mechanisms and potential long-term tissue effects.

**Key Words:** gadolinium-based contrast agents, rat, kidney, gadolinium presence, laser ablation–inductively coupled plasma–mass spectrometry, matrix-assisted laser desorption/ionization mass spectrometry imaging

(*Invest Radiol* 2026;00:000–000)

Gadolinium-based contrast agents (GBCAs) are of proven value for clinical magnetic resonance imaging (MRI).[1,2] These agents are based on the paramagnetic ion gadolinium ($Gd^{3+}$), which in its free ionic form is toxic and is therefore complexed with organic ligands to render it safe for clinical application. Depending on the structure of the ligand, GBCAs are classified as either linear or macrocyclic compounds.[3] Although they are among the safest classes of drugs, some safety concerns have emerged over time related primarily to a potential release of Gd from the chelate.[1,2,4,5]

In 2006, cases of nephrogenic systemic fibrosis were diagnosed in patients with end-stage renal disease who had been administered linear GBCA.[6–8] In 2014, increased signal intensity was observed on native $T_1$-weighted magnetic resonance (MR) images of the central nervous system in patients with normal kidney function who, months to years prior, had received repeated administrations of linear GBCA.[9,10] Ensuing research detected Gd in the brain as well as other tissues and revealed a class-dependent effect of Gd retention.[11–16] The higher retention of Gd from linear GBCAs has been linked to the differences in complex stability between the two classes, with the macrocyclic GBCAs being more stable.[17–20] In 2017, these findings led the European Medicines Agency to restrict or suspend the use of multipurpose linear GBCAs, while macrocyclic GBCAs remained approved.[21]

With many studies focusing on Gd presence in the nervous system, bone, and skin, other organs remain underexplored. Following administration, GBCAs distribute rapidly in the extracellular space and are almost exclusively excreted through the kidneys, with ~90% elimination within 24 h.[22] GBCAs are freely filtered in the glomeruli. Since there is no specific pathway ("transporter") for their reabsorption in the tubules, they are concentrated in the tubular fluid, due to tubular water reabsorption.[22] As a consequence, GBCA concentration in the final urine will on average be about 100-fold higher than in the blood plasma.[23] Interestingly, the amounts of urinary GBCA excreted by patients have enabled GBCA residue detection in urban water systems and surface waters downstream from urban areas,[24–26] serving as anthropogenic markers of health care infrastructure.

Received for publication August 10, 2026; and accepted for publication, after revision, September 18, 2026.

From the Institute of Translational Physiology, Charité – Universitätsmedizin Berlin, Germany (L.H., E.S.); MR and CT Contrast Media Research, Bayer AG, Berlin, Germany (J.B., H.P.); Max-Delbrück-Center for Molecular Medicine in the Helmholtz Association (MDC), Berlin Ultrahigh Field Facility (B.U.F.F.), Berlin, Germany (T. G., E.T., T.N.); Bioanalytics, Bayer AG, Wuppertal, Germany (A.T.).

Conflicts of interest and sources of funding: This work was supported in part by Bayer AG.

Correspondence to: Erdmann Seeliger, MD, Institute of Translational Physiology, Charité – Universitätsmedizin Berlin, Charitéplatz 1, Berlin 10117, Germany. E-mail: erdmann.seeliger@charite.de.

Supplemental Digital Content is available for this article. Direct URL citations are provided in the HTML and PDF versions of this article on the journal's website, www.investigativeradiology.com.

Copyright © 2026 The Author(s). Published by Wolters Kluwer Health, LLC. This is an open access article distributed under the terms of the Creative Commons Attribution-Non Commercial-No Derivatives License 4.0 (CCBY-NC-ND), where it is permissible to download and share the work provided it is properly cited. The work cannot be changed in any way or used commercially without permission from the journal.

ISSN: 1536-0210
DOI: 10.1097/RLI.0000000000001316

As the primary organ of excretion, it may not surprise that, following administration of high doses of GBCA in rats, high residual Gd concentrations have been detected in the kidney. Studies analyzing homogenized rat organs by inductively coupled plasma–mass spectrometry (ICP-MS) found residual Gd concentrations in the kidney 100- to 1000-fold higher than in any other investigated organ.[27–32] The decrease in renal Gd over time, resulting from continued elimination, has been reported to be more thorough following macrocyclic GBCAs,[29] resulting in higher renal Gd levels following the linear agents.[29,31]

More recent studies employed laser ablation (LA) coupled with ICP-MS to examine the spatial distribution of Gd in renal tissue slices. One study analyzed a total of 4 kidneys of rats receiving one linear or one macrocyclic GBCA at 3 and 12 months after the last administration.[33] Another study analyzed Gd concentrations in a total of 8 rat kidneys 52 days after administration of high doses of 3 macrocyclic or 1 linear GBCA.[27] Both studies observed differences between the renal cortex and the medulla; however, these observations were inconsistent. Besides the differences in the GBCA doses applied, this may rely on different time points after GBCA administration, showing snapshots of momentary Gd distribution in a process of continued elimination.

The primary aim of the present study was to provide a quantitative analysis of the intricate spatial distribution of Gd within the kidney by means of LA-ICP-MS. Previous studies investigating renal Gd distribution have typically examined a limited number of GBCAs with small sample sizes and/or focused on later time points after administration. We therefore measured Gd in renal tissue slices obtained from a larger cohort of rats receiving one of 3 macrocyclic GBCAs or one of 3 linear GBCAs at both an early and a late time point after GBCA administration. To objectively allocate Gd to the layers of the kidney, we implemented a new automated model of subsegmentation.

The chemical forms in which Gd is retained in the body remain the subject of ongoing research. Gd may reside as the intact GBCA chelate or, following dissociation, bound to endogenous ligands in either water-soluble or insoluble forms, which can be further differentiated between larger macromolecular or smaller species.[34,35] Whereas several approaches for Gd speciation have been applied to analyze Gd residues in the brain,[36–39] data on renal Gd remain limited. Initial studies have employed chromatographic separation or EPR spectroscopy to differentiate between Gd species. The results revealed that multiple macrocyclic GBCAs were largely retained as soluble intact chelates, while linear GBCAs showed predominantly insoluble Gd species.[27,33]

To gain further insight into the Gd species in the kidney, the present study approached speciation using 2 complementary modalities. As different Gd species exhibit distinct magnetic relaxation properties,[27,39,40] we first analyzed *ex vivo* kidneys by MRI. Second, we investigated the spatial distribution of intact complexes of the administered GBCAs using matrix-assisted laser desorption/ionization mass spectrometry imaging (MALDI-MSI). Together with the mapping of elemental Gd, these complementary methods provide a comprehensive view of the localization and chemical nature of renal GBCA residues. By elucidating the temporal and spatial details of both elemental Gd and intact GBCA retention across different agents, this study aimed to take a step toward linking GBCA residues to specific renal structures and to contribute to a better understanding of the underlying retention and elimination processes.

## MATERIALS AND METHODS

### Animals and treatment

A total of 70 male Han-Wistar rats (Crl:WI; body mass: 250 to 300 g) were obtained from Charles River Laboratories (Sulzfeld, Germany). All investigations were approved by the local Animal Welfare authority in accordance with the German Animal Protection Law, and the experiments were carried out in accordance with the approved guidelines. The animals were kept under standard laboratory conditions, and food and water were provided *ad libitum*.

In this exploratory study, rats were randomly assigned to 7 groups (n = 10 per group) and administered either a macrocyclic GBCA [Gadobutrol (Gadovist; Bayer AG, Leverkusen, Germany), Gadoterate (Dotarem; Guerbet, Villepinte, France), or Gadoteridol (ProHance; Bracco, Milan, Italy)], a linear GBCA [Gadobenate (MultiHance; Bracco, Milan, Italy), Gadodiamide (Omniscan; GE Healthcare, Chicago, IL), or Gadopentetate (Magnevist; Bayer AG, Leverkusen, Germany)], or isotonic saline (control; B. Braun, Melsungen, Germany). Each animal received 8 intravenous injections of 0.6 mmol Gd/kg body weight (equivalent to the human standard dose normalized to body surface area[41]) over 2 weeks (4 consecutive days per week), corresponding to a cumulative dose of 4.8 mmol Gd/kg, or volume-matched saline solution. After a resting period of either 5 days or 14 weeks, 5 rats per group were euthanized by exsanguination under 1.5% isoflurane anesthesia (Baxter, Unterschleißheim, Germany) and kidneys were harvested. Left kidneys were fixed in 4% paraformaldehyde (PFA; VWR, Darmstadt, Germany) and stored at room temperature. Right kidneys were embedded in Tissue-Tek OCT compound (Sakura Finetek, Alphen aan den Rijn, Netherlands), snap-frozen in isopentane with dry ice, and stored at −20 °C until further preparation.

### Laser Ablation–Inductively Coupled Plasma–Mass Spectrometry

To prepare samples for LA-ICP-MS, frozen kidneys were subject to cryosectioning in coronal orientation (CM1950, Leica Biosystems GmbH, Nussloch, Germany). Tissue slices of 10 µm thickness from the central plane were collected on glass slides and briefly dried at 37 °C. The remainder of the kidneys was stored at −20 °C. In the kidney slices, the spatial distributions of the element Gd were determined using a LA system (NWR 213; New Wave Research, Fremont, CA) coupled to an ICP-MS (iCAP RQ ICP-MS, Thermo Fisher Scientific, Bremen, Germany). LA was performed as previously described in detail.[42] Briefly, continuous-line ablation mode was employed, and the laser energy was optimized daily to attain ~3 J/cm$^2$, which led to complete local ablation of the sample material. The ablation spot size was 40×40 µm with no distance between lines. The laser frequency was 50 Hz and the scan speed 400 µm/s, which resulted in a pixel dimension of 20×40 µm. The ablated tissue material was transferred to the ICP-MS by a constant flow of helium (900 mL/min), and the isotope $^{158}$Gd was measured. Gelatin standards with defined Gd concentrations (0.0, 1.1, 21.7, 53.9 and 0.0, 60.9, 526.6, 5343.5 nmol/g) were used as previously described to construct calibration curves and limits of detection (LOD).[42] Images visualizing the spatial distribution of Gd within the kidney slices were generated using the software ImaJar 3.63b, generously provided by R. Schmid and U. Karst (University of Münster, Germany).


Copyright © 2026 The Author(s). Published by Wolters Kluwer Health, LLC.

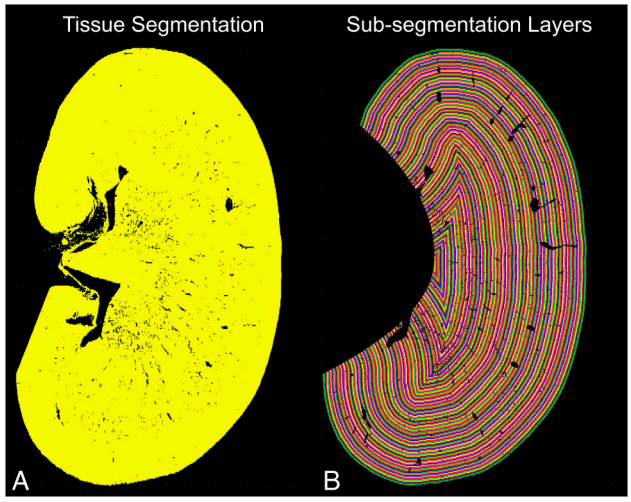



**FIGURE 1.** Illustration of the renal segmentation used to calculate the Gd content (A) and of the sub-segmentation with pixel-wide layers used to generate Gd depth profiles (B). Gd, gadolinium.

## Mapping of Renal Gadolinium Concentration

To separate kidney tissue from background, we applied the automated bean shape model for renal segmentation[43] (Fig. 1A). This facilitated the calculation of the mean Gd concentration across all pixels of each individual kidney slice (hereinafter referred to as Gd content). For the quantification of the intrarenal spatial distribution of Gd, sub-segmentation of the kidney is required. The kidney consists of 3 anatomic layers: the cortex, the outer medulla, and the inner medulla. Because the rather broad transition zones between these 3 renal layers contain histologic structures of both adjacent anatomic layers in immediate proximity, the transition zones are often excluded in renal sub-segmentation models, particularly for analysis of MRI.[44,45] This approach turned out unsuitable for our present data, since we observed particular Gd distribution patterns including these transition zones. We, therefore, developed a multilayered sub-segmentation defining single-pixel-width concentric layers starting at the renal capsule and progressing inward toward the inner medulla (Fig. 1B). We excluded the renal pelvis and the papilla from this sub-segmentation in the form of a parabolic cutout. To normalize kidney sizes varying between 137 and 174 pixel-wide layers, the number of layers was interpolated to 150 standardized layers. From these 150 layers, mean Gd concentrations per layer were calculated and individual depth profiles of Gd concentrations were generated. From these data, descriptive statistics (mean ± SD) per GBCA group of the individual depth profiles were calculated. Finally, distinguishing between concentric layers corresponding to either the renal cortex or the medulla, layers with the highest average Gd concentration were identified for each GBCA.

## *Ex Vivo* Magnetic Resonance $T_1$ Relaxometry

From the kidneys that had been immersed in 4% PFA, 2 per group and time point were randomly selected for MR $T_1$ relaxometry. The kidneys harvested 5 days after the last GBCA administration had been stored in PFA for 18 weeks before the kidneys and some of the surrounding fixative were transferred to 5 mL Eppendorf cups for MR analysis. For MRI data acquisition, the cups were placed in a 2-channel volumetric transceiver RF coil on a 9.4 T animal MR scanner (BioSpec, Bruker BioSpin, Ettlingen, Germany). $T_1$ mapping was performed with a rapid acquisition with refocused echoes (RARE) technique: echo time (TE) = 9.87 ms, repetition time (TR) array = 100, 170, 250, 336, 435, 550, 685, 848, 1060, 1353, 1843 and 3750 ms, RARE factor = 2, slice thickness = 0.4 mm, field of view (FOV) = 24 × 24 mm, matrix = 480×480, resolution 50×50 µm, number of averages = 9 and total acquisition time = 9 hours 48 minutes 41 seconds for each $T_1$ map. Quantitative visualization, segmentation, and validation were performed using in-house developed software based on MATLAB and ImageJ.

## Matrix-assisted Laser Desorption Ionization–Mass Spectrometry Imaging

For MALDI-MSI analysis, we selected gadobutrol and gadodiamide as examples for macrocyclic and linear GBCAs, respectively. We used the remaining kidney tissues from LA-ICP-MS analysis. With an offset from the central plane slices used for the LA-ICP-MS measurements, coronal tissue slices of 10 µm were collected from these samples and mounted on conductive indium-tin-oxide–coated slides (Bruker Daltonics, Bremen, Germany) and stored at −80 °C. For MALDI-MSI analysis, slides were thawed inside a desiccator and subjected to a chloroform wash: 2×30 second horizontally under gentle shaking inside a glass Petri dish. An internal standard for quantification (holmium butrol, 0.75 µg/mL) in 80% acetonitrile and a 1,5-diaminonaphthalene matrix (10 mg/mL) in 70% acetonitrile were applied to kidney slices consecutively using an HTX M5 automated sprayer (HTX Technologies, Chapel Hill, NC) at concentrations of 19 pg/mm$^2$ and 2.6 µg/mm$^2$, respectively. MALDI-MSI was performed with a scimaX 7T FT-ICR (Bruker Daltonics, Bremen, Germany) using a step size of 40 µm, the medium focus setting with 35% laser power, and 200 shots at 800 Hz with a mass resolution of ~200k (full width at half maximum) at a mass-to-charge ratio (*m*/*z*) of 400. Data were recorded from *m*/*z* 150 to 900 with continuous accumulation of selected ions (*m*/*z* 600 ± 50) with internal mass calibration. LOD and calibration curves for quantification were constructed from spiked naive rat kidney homogenate[46] (Supplemental Digital Content Fig. 1, Supplemental Digital Content 1, https://links.lww.com/RLI/B145). Ion images were normalized to the internal standard for quantification or the total ion count (SCiLS Lab Pro MVS 2025b, Bruker Daltonics, Bremen, Germany). Subsequently, tissue slices directly adjacent to those analyzed by MALDI-MSI were analyzed for their elemental Gd distribution by LA-ICP-MS.

## High-performance Liquid Chromatography Analysis

A high-performance liquid chromatography (HPLC) system (Agilent 1290 Infinity II, Waldbrunn, Germany) with a column (Thermo Hypercarb 100×3.0 mm 5 µm, Thermo Scientific, Dreieich, Germany) was connected to an ICP-MS (Agilent 7900, Waldbrunn, Germany) and employed as previously described[19,47] to explore Gd species present in the PFA supernatant of submerged rat kidneys from random exemplary samples of the gadobutrol and gadopentetate groups. 10 to 20 µL aliquots of the PFA, as well as dilutions ranging from 1:2 to 1:10, were analyzed and compared with 10 µM solutions of the respective GBCA. The signal intensities of the $^{158}$Gd isotope were recorded and displayed as chromatograms.

## Statistical Analysis

Descriptive statistics and statistical analyses were performed and graphs generated using GraphPad Prism 10 (Version 10.6.1, GraphPad Software LLC., Boston, MA).

*Copyright © 2026 The Author(s). Published by Wolters Kluwer Health, LLC.*

## RESULTS

### Mapping of Gadolinium by Laser Ablation–Inductively Coupled Plasma–Mass Spectrometry

A total of 68 rat kidneys were successfully sectioned and analyzed to map residues of the administered GBCAs. Spatial maps of renal Gd distribution generated from LA-ICP-MS data obtained from kidneys harvested 5 days after the last GBCA administration showed that Gd was predominantly localized in the renal cortex, with 10- to 100-fold lower medullary levels across all administered GBCAs (Fig. 2A). No obvious differences in the distribution patterns and concentration ranges were observed within and between the classes of macrocyclic and linear GBCAs.

Gd presence after an additional 13 weeks of excretion, that is, at week 14 p.i., showed cortical Gd levels about 2 orders of magnitude lower and medullary concentrations about one order of magnitude lower compared with the early time point (day 5 p.i.). Among all 6 GBCAs, gadodiamide stood out with the most residual Gd while gadoteridol showed the least. Moreover, distinct changes in the spatial distribution patterns of Gd (Fig. 2B) were observed. With the exception of gadobenate, all GBCAs showed a layered Gd distribution differing from that observed at day 5 p.i.: elevated Gd levels in the cortex, minimal levels in the transition zone from cortex to outer medulla, increasing levels in the outer medulla reaching highest levels in the transition zone between outer and inner medulla, and declining levels in the inner medulla. This distribution pattern showed a prominent arc of Gd presence at the transition zone between outer and inner medulla, following a concentric ellipsoidal pattern similar to the renal capsule. Following gadobenate, Gd remained predominantly in the cortex with only sparse medullary presence.

Descriptive statistics for the Gd content (the mean concentrations across all pixels per slide) are illustrated in Figure 3. At day 5, the Gd content ranges were comparable among the GBCAs (group median ranging from 918 to 2361 nmol/g) with the exception of gadobenate (median: 751 nmol/g). At week 14, no substantial differences were observed among the GBCA groups (group median ranging from 1.2 to 13.3 nmol/g), with the exception of gadodiamide (median: 83 nmol/g). Within each GBCA group, remaining Gd concentrations at week 14 were significantly lower than at day 5 ($P < 0.05$ for all GBCA groups). A considerable interindividual variability was observed within most of the groups at both time points. We therefore elected not to apply statistical tests to assess possible differences among the groups. In contrast to the other GBCAs that are excreted almost completely through the kidneys, gadobenate is, in addition, excreted through the liver to an extent of around 50% in rats.[48] Considering the heterogeneity within the 2 classes of GBCAs, including the dual elimination route of gadobenate and differences in their ionic character, we also refrained from statistical testing for possible differences between the two classes. In kidney tissue from rats receiving saline solution, Gd was below the LOD (LOD ≤1.1 nmol/g).

The spatially resolved Gd concentration data were applied to generate depth profiles of renal Gd, representing the different Gd distribution patterns (Fig. 4), and to determine the Gd concentrations in those concentric layers in which peak concentrations within the cortex and the medulla were measured (Table 1). For all administered GBCAs, the quantitative depth profiles at day 5 showed high Gd concentrations in the cortex with a steep decline at the corticomedullary transition zone and 10- to 100-fold lower concentrations throughout the medulla, with the highest concentrations in the transition zone between the outer and inner medulla. Within the cortex, peak

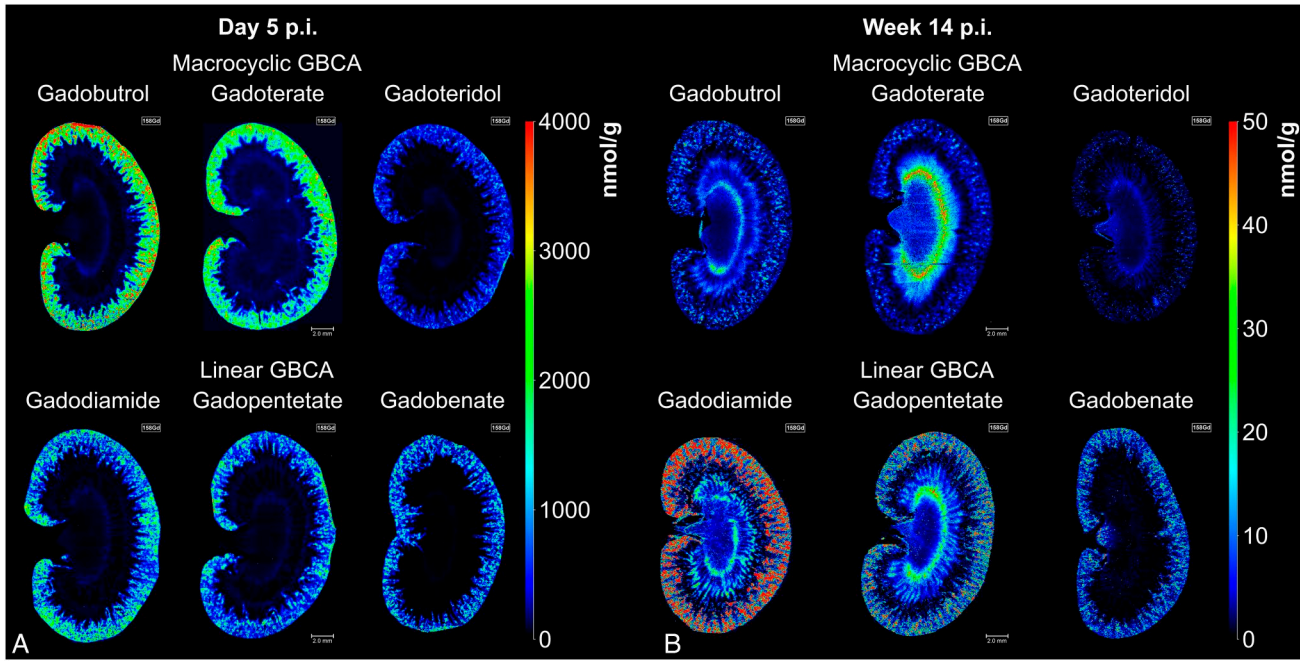



**FIGURE 2.** Quantitative Gd distribution obtained by LA-ICP-MS: representative examples for each GBCA at day 5 (A) and week 14 (B); resolution 40×40 µm. Each map represents the sample with median Gd concentration across all pixels per slice for the respective GBCA group. Color scales indicate Gd concentrations, ranging up to 4000 nmol/g (A) and 50 nmol/g (B). GBCA, gadolinium-based contrast agent; Gd, gadolinium; LA-ICP-MS, laser ablation–inductively coupled plasma–mass spectrometry.


Copyright © 2026 The Author(s). Published by Wolters Kluwer Health, LLC.

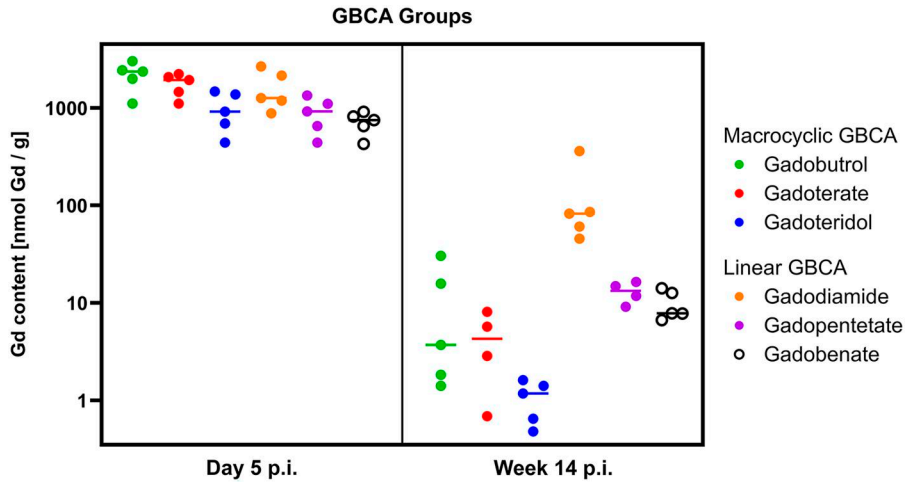



**FIGURE 3.** Gd concentration across all pixels per kidney slice for each GBCA at day 5 and at week 14 p.i. Data are presented as individual values with group median on a logarithmic scale. Because of its additional hepatobiliary elimination, individual values for gadobenate are illustrated as circles, instead of dots. GBCA, gadolinium-based contrast agent; Gd, gadolinium.

concentrations were always detected in the third or fourth outermost layer of the 150 concentric layers generated, which located them close to the renal capsule. Medullary peak concentrations were detected between layers 108 and 116, corresponding to the transition zone between the outer and the inner medulla. For all GBCAs, peak concentrations were higher in cortical than medullary layers.

Comparison of the quantitative depth profiles of Gd at week 14 versus day 5 confirmed the changes in the distribution pattern shown by the Gd maps (Fig. 4; Table 1). For most GBCAs, the depth profiles revealed elevated Gd concentration in the cortex, a decline to minimal levels in the corticomedullary transition zone, a second elevation within and around the transition zone between the outer and inner medulla reaching levels comparable to the cortex, and a gradual decline in the inner medulla. One kidney in the gadodiamide group showed 3- to 4-fold higher cortical Gd concentrations than the other 4 kidneys of this group resulting in a large SD in this group, however, even in the other 4 gadodiamide kidneys, cortical Gd concentrations were higher than in all kidneys of the other GBCA groups. Cortical peak concentrations were mostly determined at concentric layers 5 to 7, close to the renal capsule, except for gadoteridol, which exhibited a broader plateau spanning layers 10 to 25, corresponding to most of the cortical area. Medullary peak concentrations were measured at layers 103 to 111, corresponding to the transition zone between outer and inner medulla. Notably, these medullary peaks were substantially more pronounced than at 5 days, consistent with the concentric ellipsoidal arc pattern observed in the Gd distribution maps from several GBCAs (Fig. 2B). While linear GBCAs showed highest peak concentrations in cortical layers, macrocyclic GBCAs in general displayed highest peak concentrations in medullary layers at this time point.

## Assessment of Gadolinium-based Contrast Agent Residues by Magnetic Resonance Relaxometry

For *ex vivo* MRI analyses, kidneys were immersed and stored in a 4% PFA solution. In kidneys obtained 5 days after the last administration of GBCAs (n = 2 per group) or saline (control), $T_1$ relaxation times were determined by parametric $T_1$ mapping

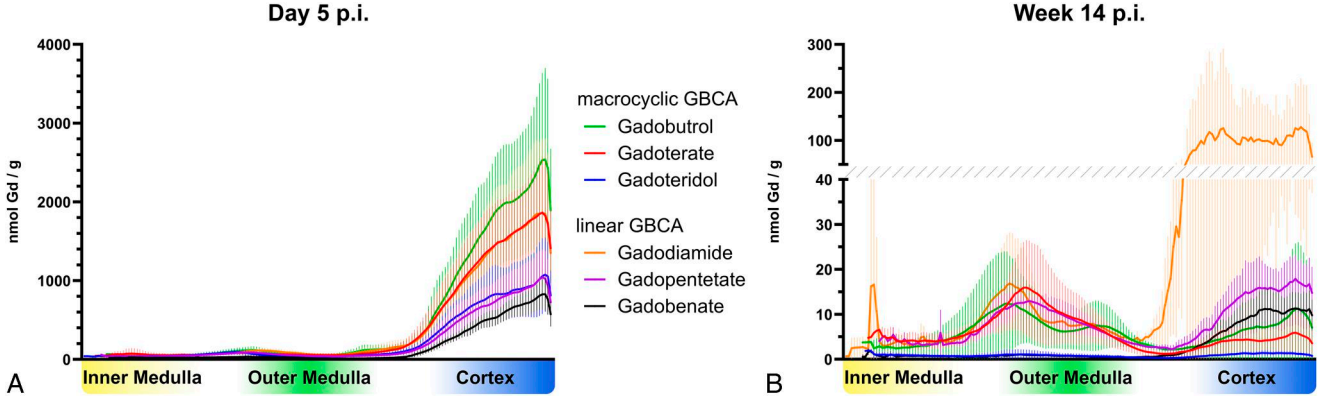



**FIGURE 4.** Depth profiles of Gd concentration derived from concentric sub-segmentation of LA-ICP-MS data for each GBCA at day 5 (A) and at week 14 p.i. (B). Data are presented as group means ± SD. Color-coded labels along the *x*-axis indicate the approximate location of the cortical and medullary regions. The *y*-axis for week 14 includes a break, with the upper range displaying a larger Gd concentration range. GBCA, gadolinium-based contrast agent; Gd, gadolinium; LA-ICP-MS, laser ablation–inductively coupled plasma–mass spectrometry.

*Copyright © 2026 The Author(s). Published by Wolters Kluwer Health, LLC.*

**TABLE 1.** Peak Gd Concentrations in Cortical and Medullary Regions at 5 Days and 14 Weeks p.i. Values Represent Highest Group Mean ± SD Among the 150 Concentric Layers

| | Peak Gd (nmol/g) at 5 d p.i. | | | | Peak Gd (nmol/g) at 14 wk p.i. | | | |
|---|---|---|---|---|---|---|---|---|
| **Group** | **Medullary** | | **Cortical** | | **Medullary** | | **Cortical** | |
| Macrocyclic | | | | | | | | |
| Gadobutrol | 119.6 | ± 46.5 | 2538.0 | ± 1163.4 | 12.4 | ± 11.5 | 11.3 | ± 14.8 |
| Gadoterate | 82.6 | ± 9.8 | 1865.0 | ± 705.8 | 16.0 | ± 10.6 | 5.9 | ± 4.8 |
| Gadoteridol | 92.1 | ± 34.4 | 1076.4 | ± 469.9 | 2.0 | ± 0.0 | 1.4 | ± 0.6 |
| Linear | | | | | | | | |
| Gadodiamide | 115.7 | ± 28.5 | 1862.9 | ± 938.8 | 16.9 | ± 11.3 | 127.9 | ± 101.5 |
| Gadopentetate | 87.6 | ± 19.1 | 1042.7 | ± 350.9 | 13.0 | ± 1.1 | 17.9 | ± 5.3 |
| Gadobenate | 34.2 | ± 8.7 | 828.22 | ± 205.0 | 1.8 | ± 0.5 | 11.3 | ± 3.6 |

Gd, gadolinium.

(Fig. 5, Supplemental Digital Content Table 1, Supplemental Digital Content 3, https://links.lww.com/RLI/B147). The average $T_1$ relaxation times of the saline control kidneys amounted to 451 ms in the cortex, 707 ms in the outer medulla, and 1152 ms in the inner medulla. $T_1$ shortening was found in the kidneys of all GBCA groups: For all linear GBCA kidneys, $T_1$ ranged from 251 to 281 ms, from 354 to 579 ms, and from 491 to 721 ms; for all macrocyclic GBCA kidneys, $T_1$ ranged from 385 to 417 ms, from 604 to 648 ms, and from 864 to 928 ms, in the cortex, outer medulla, and inner medulla, respectively. However, next to $T_1$ shortening in the tissue of kidneys of all GBCA groups, we also observed $T_1$ shortening in the surrounding PFA (Fig. 5), indicating substantial washout from the renal tissue. An exploratory analysis of the surrounding PFA from kidneys following macrocyclic gadobutrol and linear gadopentetate by HPLC detected Gd almost exclusively in the form of the intact GBCAs (Fig. 5). LA-ICP-MS of exemplary PFA-fixed kidneys further supported this by revealing significantly less Gd than in the native, snap-frozen contralateral kidneys (Supplemental Digital Content Fig. 2, Supplemental Digital Content 2, https://links.lww.com/RLI/B146).

## Mapping of Intact Gadolinium-based Contrast Agents by Matrix-assisted Laser Desorption Ionization–Mass Spectrometry Imaging

In contrast to LA-ICP-MS, MALDI-MSI detects the intact chelate. Signal intensities in MALDI-MSI are strongly dependent on the ionizability of the analyte as well as suppression effects exerted by the sample. Consequently, a MALDI-MSI method needs to be established for each GBCA individually. The distribution of intact chelates was only determined for the macrocyclic gadobutrol (LOD = 1.0 nmol/g) and the linear gadodiamide (LOD = 9.4 nmol/g) by MALDI-MSI. At day 5, most of the intact gadobutrol was detected in the renal cortex (Fig. 6A, left). At week 14, intact gadobutrol was detected mostly in the medulla and sparsely in the cortex (Fig. 6B, left). Direct comparison with elemental Gd as measured by LA-ICP-MS revealed almost identical distribution patterns (Figs. 6A, B, right). For the linear gadodiamide, at day 5, most of the intact chelate was located at the cortex (Fig. 6C, left), which agreed with the distribution pattern of elemental Gd (Fig. 6C, right). At week 14, however, MALDI-MSI could not detect intact chelate of gadodiamide.

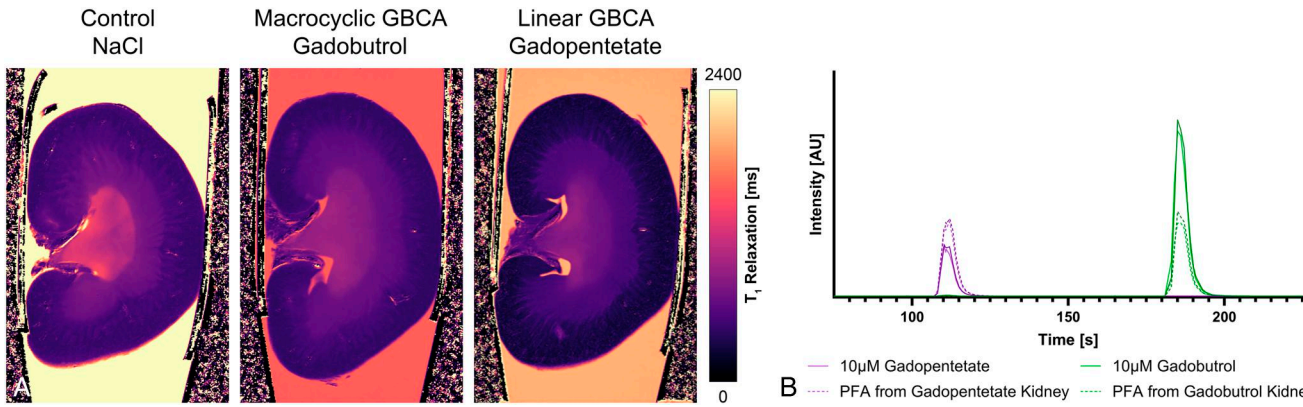



**FIGURE 5.** $T_1$ maps of PFA-immersed kidneys obtained by MR scanning (A): representative examples of *ex vivo* kidneys from control, macrocyclic GBCA, and linear GBCA groups at day 5 p.i.; resolution 50×50 µm. The color scale indicates $T_1$ relaxation ranging up to 2400 ms. Chromatograms from HPLC analysis (B) of the representative PFA supernatant (dotted lines) and the respective GBCA standard (solid lines): the signal intensity for Gd in AU is plotted vs. retention time in seconds. AU, arbitrary units; GBCA, gadolinium-based contrast agent; Gd, gadolinium; HPLC, high-performance liquid chromatography; MR, magnetic resonance; PFA, paraformaldehyde.


Copyright © 2026 The Author(s). Published by Wolters Kluwer Health, LLC.

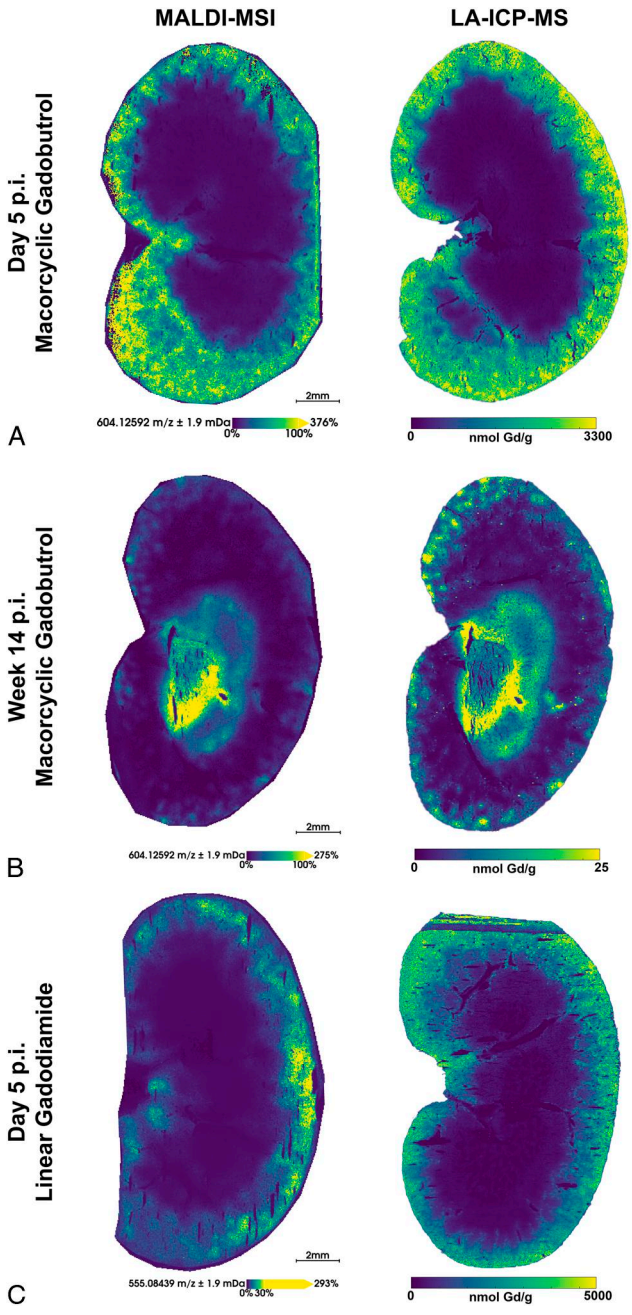



**FIGURE 6.** Distributions of intact GBCA chelates obtained by MALDI-MSI (left 3) together with the distribution of Gd obtained by LA-ICP-MS (right 3) within the same kidneys: gadobutrol at day 5 p.i. (A) and at week 14 p.i. (B), gadodiamide at day 5 p.i. (C); resolution 40×40 µm. Color scales of MALDI-MSI images are not directly indicative of concentration but signify the relative presence of gadobutrol and gadodiamide, identified by their mass-to-charge ratio *m/z*: gadobutrol = $[M\text{-}H]^-$ *m/z* 604.12592, gadodiamide = $[M\text{-}H\text{-}H_2O]^-$ *m/z* 555.08439. Color scales of LA-ICP-MS images indicate Gd concentrations. GBCA, gadolinium-based contrast agent; Gd, gadolinium; LA-ICP-MS, laser ablation–inductively coupled plasma–mass spectrometry; MALDI-MSI, matrix-assisted laser desorption ionization–mass spectrometry imaging.

## DISCUSSION

In this study, we systematically investigated the spatial distribution of residues from multiple macrocyclic and linear GBCAs in the rat kidney. Our analysis consisted of 3 modalities. The distribution of elemental Gd was examined and quantified using LA-ICP-MS. MR-detectable GBCA residues were assessed by MR relaxometry. For gadobutrol and gadodiamide, the distribution of intact GBCA chelates was determined by MALDI-MSI. All 3 modalities analyzed whole kidney tissue slices or intact kidneys, providing an advantage over homogenized kidney tissue. Our results revealed nonhomogeneous distribution patterns, which changed differently for linear versus macrocyclic GBCAs over the course of their elimination from day 5 to week 14. We corroborated earlier observations, revealed distinct spatial and temporal distribution patterns not previously described, and proposed how particularities of intrarenal architecture and physicochemical conditions may influence GBCA retention in the kidney.

The present study is the first to analyze residual renal Gd content from multiple linear and macrocyclic GBCAs at a time point as early as day 5 post administration. We observed similar renal Gd content across the GBCAs with the exception of gadobenate, which showed the lowest median Gd content, most likely due to its additional hepatobiliary excretion route (around 50% in rats[48]). The overall magnitude of Gd retention at day 5 was comparable to findings reported from homogenized kidney tissue at day 7 following GBCA administration.[28,29,31,32] One of these studies reported a 2- to 4-fold higher renal Gd content for linear versus macrocyclic GBCAs.[31] Because the cumulative GBCA dose applied in this previous report was about 10-fold higher than in the present study, it is conceivable that class-based differences at early time points may only emerge at higher cumulative doses.

Major elimination of GBCA residues took place between day 5 and week 14 in all GBCA groups. The present data on Gd content at week 14 are in line with reports from homogenized or partially dissected kidneys at comparable time points.[27–29] The vast majority of earlier *in vivo* studies on GBCA residues in various organs focused on the comparison between macrocyclic and linear GBCAs, rather than within the two classes, and typically reported significantly lower residues following macrocyclic than linear GBCAs.[27,30,31,39,49] The present data on GBCA residues in the kidney are less clear-cut. First, the gadodiamide group showed a Gd content about one order of magnitude higher than the other linear GBCAs, indicating heterogeneity within this class. This is in line with a report on the *in vitro* stability of GBCA chelates in human blood serum.[19] This study found the release rate of Gd from its chelate for the nonionic linear gadodiamide about 10-fold higher than for the ionic linear agents gadobenate and gadopentetate. These results, in conjunction with those of the present *in vivo* study, indicate that the ionic character may play a role in Gd retention within the class of linear GBCAs. Second, the renal Gd content of the other 5 GBCA groups, that is, the 3 macrocyclic and the 2 remaining linear GBCAs, showed no substantial differences. This does not agree with the human serum study, in which macrocyclic GBCAs showed no detectable release of Gd, in contrast to the linear agents.[19] However, the GBCA residues found following *in vivo* administration are not limited to released Gd, but are known to occur in the form of intact GBCAs as well.[35,50] Moreover, human serum is devoid of cells

*Copyright © 2026 The Author(s). Published by Wolters Kluwer Health, LLC.*

and extracellular matrix, which potentially play a key role in GBCA retention *in vivo*, particularly in the kidney with its unique microanatomy and physicochemical environment.

The interindividual variability within almost all GBCA groups at both time points appeared unusually large when compared with various structural and functional parameters documented for the kidney of healthy rats in the literature. However, similar data on interindividual variability of renal Gd concentrations have been reported in previous rat studies.[27,31,32] Given the high standardization regarding the rat models and analytic procedures within each of these studies, the reason behind this variability remains elusive. Because of the high variability and because of heterogeneity within classes, such as the differences in ionic character and the dual elimination route of gadobenate, we elected not to compare the 6 groups or the 2 classes of GBCAs using a statistical approach.

Our data on spatial distribution of Gd provided more detailed insights into renal Gd presence and may help to identify histologic structures and mechanisms of renal retention. At day 5, we observed similar distribution patterns for all investigated GBCAs: the vast majority of Gd resided in the renal cortex. All groups showed peak Gd concentrations in the cortex 1 to 2 orders of magnitude greater than in the medulla. This difference between cortex and medulla appears to remain for around 2 more weeks, as shown in a report from partially dissected kidneys at day 17 following GBCA administration.[27]

At week 14, cortical Gd concentrations were about 2 orders of magnitude lower and medullary concentrations about one order of magnitude lower compared with day 5. While this differential elimination was observed for all GBCAs, it was most pronounced for macrocyclic agents, resulting in higher medullary than cortical Gd concentrations in this GBCA class. Notably, cortical Gd from gadodiamide was eliminated less than from all other GBCAs. Our data on spatial distribution are in line with a previously reported observation for gadobutrol and gadodiamide at week 12 following GBCA administration,[33] including the minimal Gd concentration around the corticomedullary transition zone as well as the arc of increased Gd concentration at the transition zone of the outer medulla to the inner medulla. We determined similar patterns following gadoterate, gadoteridol, and gadopentetate, which had not previously been studied. Intriguingly, in-depth inspections of the data obtained at day 5 revealed a similar concentric ellipsoidal pattern of elevated Gd in the transition zone between inner and outer medulla.

The reason behind the spatial Gd distribution pattern within the kidney and the changes of this distribution over time observed in the present study is unclear. Following their glomerular filtration, GBCAs are concentrated in the tubular fluid along the tubules, such that in the fluid within the final segment of the nephron, the collecting duct in the deepest layers of the inner medulla, GBCA concentrations will be about 100-fold higher than in the blood plasma. However, the relatively short plasma half-life of GBCAs[22] in conjunction with the spatial distribution of the residues observed 5 days after their last administration—with the deepest layers of the inner medulla among the renal regions with the lowest Gd concentrations—rules out that, at this time point and beyond, the tubular fluid still contains residues in substantial concentrations. Within the given time frame, GBCAs must have already been virtually completely flushed out of the nephron with the final urine. Thus, the high concentrations of renal Gd and its spatial distribution observed here must rely on other distinctive features of the kidney. These include the particular vascular architecture of the distinct renal layers, the structurally and functionally highly differentiated nephron segments that are formative for these layers, and the particular physicochemical conditions within the renal tissue and its differences among the layers.

Based upon an anecdotal report indicating that Gd may be prominently retained in the wall of intrarenal blood vessels, particularly in their middle coat (tunica media),[51] which is thickest in arteries,[52] Bücker et al[33] postulated that the major portion of the retained Gd would reside in the walls of intrarenal arteries. By means of LA-ICP-MS, these authors located the majority of residual Gd in rat kidneys 12 weeks post-GBCA within and around the transition zone between the outer and inner medulla. While this distribution pattern agrees well with the pattern we observed 14 weeks post-GBCA, the architecture of intrarenal arteries contradicts the authors' assumption. The density of arteries in the medullary tissue is rather low, with only 6 to 10 interlobar arteries traversing the rat medulla.[53–55] The highest density of arteries is found first within the corticomedullary transition zone containing the arcuate arteries, and second within the cortex, particularly in its deeper portions, that contain the interlobular arteries.[53,55,56] At day 5 post-GBCA, we measured the vast majority of Gd in the renal cortex. Intriguingly, Gd concentrations were not consistent across the whole cortex: they were highest close to the renal capsule and declined steadily throughout the cortex, with the lowest values in its deepest portions. This is inverse to the gradient in density of cortical arteries,[53,55] which further contradicts the notion that major portions of the retained Gd reside in the walls of intrarenal arteries.

The most probable structures responsible for the distinct intrarenal distribution pattern at day 5 are tubular epithelial cells. Several studies found GBCA residues in vacuoles in the epithelium of the proximal tubule.[57–60] Our finding that the highest Gd concentrations within the cortex were located close to the renal capsule probably relies on the fact that this is the area with the highest density of proximal tubules.[53,54] As shown for a variety of other substances including, but not limited to, iodinated x-ray contrast agents and dextran, these vacuoles are formed by endocytic uptake and can fuse with lysosomes, which is followed by their slow reduction over days to weeks.[60,61] This process of transient storage has not been associated with impairment of tubular function.[57,60–63] The transient character of this storage has also been shown for GBCAs,[57,58,60] which explains the 10- to 100-fold lower cortical Gd presence at week 14 as compared with day 5.

The reason behind the localized Gd presence within and adjacent to the transition zone between the outer and inner medulla that we observed at week 14 and even at day 5 and that Bücker et al[33] also observed at week 12 is unclear. With regard to histologic structures that may host substantial amounts of residual Gd in this area, arterial walls can be ruled out due to their low density. The tubular epithelial cells of the nephron segments located in this area, that is, thin descending and thin ascending limbs of the loop of Henle, small portions of the deepest thick ascending limbs of Henle's loop, and collecting ducts, do not form vacuoles by endocytic uptake of exogenous substances.[57–62]

We hypothesize that the elevated Gd concentrations in this area may result from the unique combination of physicochemical conditions in medullary tissue. Firstly, the medullary segments of the nephron generate high osmolalities within the interstitium of the medulla: the osmolality rises steadily from the corticomedullary border to the deepest layers of the inner medulla. Approximately half of the increase in osmolality is


Copyright © 2026 The Author(s). Published by Wolters Kluwer Health, LLC.

generated in the outer medulla that concentrates NaCl; the inner medulla generates the second half of the osmolality increase by concentrating urea.[23] Secondly, owing to the particular microvascular architecture, tissue partial pressure of oxygen ($pO_2$) and pH decline while $pCO_2$ increases steadily from the corticomedullary border to the deepest layers of the inner medulla.[23,56,64] As a result, the tissue in the transition zone between the outer and inner medulla is exposed to a combination of high NaCl concentration, high osmolality and high $pCO_2$, alongside low $pO_2$ and low pH. We speculate that this unique combination may favor retention of GBCA residues. Within the inner medulla, the physicochemical conditions change substantially as compared with the outer medulla, with the only exception of the NaCl concentration: the concentration of urea is much higher, and the osmolality and $pCO_2$ become even higher and $pO_2$ and pH even lower than in the outer medulla.[23,56] It is conceivable that this unique combination does not favor retention of GBCA residues.

While these hypotheses are consistent with our observations, they remain to be confirmed through complementary approaches. Histologic studies may confirm the proximal tubules involved in transient cortical retention, and *in vitro* studies replicating the characteristic medullary physicochemical conditions may uncover retention mechanisms at the transition zone from outer to inner medulla.

In an attempt to further assess Gd presence, kidneys fixed and stored in PFA solution were analyzed by MR relaxometry. Surprisingly, the results from LA-ICP-MS did not align with the results from MRI, as MR relaxometry indicated comparable $T_1$ shortening across all renal layers. This discrepancy most probably originated from the difference in sample preparation. Different from snap-freezing native kidneys as used for LA-ICP-MS, preparation with PFA allowed substantial washout of the GBCA residues, as indicated by the $T_1$ shortening in the surrounding PFA solution of GBCA kidneys but not of control kidneys. Therefore, sample preparation must prevent washout of these highly hydrophilic substances to preserve the presence and spatial distribution of GBCA residues. Since kidneys from week 14 p.i. had also been fixed and stored in PFA, we did not perform MR relaxometry of these kidneys. Notably, HPLC of the PFA supernatant detected the washed-out Gd almost exclusively in the form of the intact chelates, which is in line with their hydrophilic nature. The stronger $T_1$ shortening in PFA solution following macrocyclic GBCAs suggested a greater presence of the intact chelates than following linear GBCAs. The LA-ICP-MS analysis of exemplary PFA-fixed kidneys indicated lower Gd concentrations following macrocyclic GBCAs compared with linear GBCAs. A possible reason behind these findings is that the linear GBCAs—due to their lower stability—are stored in a water-insoluble species to a greater extent than macrocyclic agents.

By means of MALDI-MSI, the spatial distribution of intact GBCA was determined for gadobutrol and gadodiamide as examples of macrocyclic and linear GBCAs. LA-ICP-MS analysis of the adjacent tissue slices allowed direct comparison of the distribution patterns of intact GBCA and elemental Gd. For the macrocyclic gadobutrol, the distribution pattern of intact GBCA closely resembled that of elemental Gd at day 5 post administration. In line with our observation of GBCA "washed out" by PFA solution, this indicates that, at this early time point, Gd from gadobutrol predominantly resided in the form of the intact GBCA. Even at week 14, the spatial distribution of intact gadobutrol and elemental Gd was again found to be similar, with both showing highest levels in the medulla. This suggests that Gd still largely resided as the intact chelate. This observation is in line with a previous report suggesting that gadobutrol largely resides in its intact form in kidney tissue.[33]

The distribution pattern of the linear gadodiamide was similar to that of elemental Gd at day 5, suggesting that at this early time point, Gd from gadodiamide also predominantly resided in the form of the intact GBCA. At week 14, however, analysis of gadodiamide did not show any detectable intact chelate. Given the low LOD for the gadodiamide chelate relative to the high concentrations of elemental Gd, the majority of remaining Gd most probably does not reside in the form of the intact chelate at this time point. Earlier reports on renal Gd 1 year after last administration of gadodiamide revealed virtually no more intact chelate but only elemental Gd.[33,65]

This study has several limitations. First, while the chosen time points of 5 days and 14 weeks post-GBCA provided insights into both early retention and long-term elimination, analysis at even earlier time points (eg, 24 to 72 h) may have captured additional details of the initial distribution of the rapidly cleared GBCAs. Second, the spatial resolution of our imaging modalities was sufficient to assign Gd and GBCAs to distinct portions of the renal layers, but it did not permit identification of specific histologic structures such as the distinct segments of the nephron. Complementary histologic examination would enable us to draw conclusions on involved retention mechanisms. Third, we observed substantial interindividual variability in Gd concentrations within GBCA groups. While such variation is not typical for renal parameters, it has been reported in previous studies of renal GBCA retention and may reflect biological heterogeneity in GBCA retention or elimination. Finally, although we investigated several agents from both macrocyclic and linear GBCA classes, conclusions about other GBCAs of the 2 classes should be drawn with due caution.

Virtually all clinical and preclinical studies published so far demonstrated that renal GBCA residues do not perturb any of the various functions of the kidneys. Considering that administration of GBCA serves diagnostic rather than therapeutic purposes, it nevertheless seems worthwhile to elucidate the distinct mechanism(s) of renal GBCA/Gd retention and the factors that may favor or prevent it. As first steps, we propose histologic *ex vivo* studies to assess the role of GBCA/Gd endocytosis by cells of the proximal tubules, and *in vitro* studies modeling the specific physicochemical conditions in the renal medulla to uncover the mechanisms of GBCA/Gd retention in this layer.

In conclusion, this study provides the first comprehensive spatially resolved characterization of renal GBCA residues at an early and a late time point. We demonstrate that GBCA residues exhibit specific distribution patterns and distinct changes in these patterns over the course of their elimination. Our findings of specific retention patterns suggest that—beyond GBCA-specific differences in the stability, osmolality, and ionic character of the chelates—the unique microanatomy and physicochemical conditions in the kidney play critical roles in renal GBCA retention. These insights provide a foundation for future investigations into retention mechanisms and potential long-term tissue effects.

## ACKNOWLEDGMENTS

*The authors thank Steve Baethge, Kathrin Boettger, Claudia Heyer, Robert Ivkic, Ines Krause, and Beate Schnippert for their excellent technical assistance. The authors also thank Dr Hannes-Friedrich Ulbrich for his expertise and advice on the statistical analysis of the data.*

Copyright © 2026 The Author(s). Published by Wolters Kluwer Health, LLC. 

## REFERENCES


1. Lohrke J, Frenzel T, Endrikat J, et al. 25 years of contrast-enhanced MRI: developments, current challenges and future perspectives. *Adv Ther*. 2016;33:1–28.
2. Frenzel T, Wels T, Pietsch H, et al. Recent developments and future perspectives in magnetic resonance imaging and computed tomography contrast media. *Invest Radiol*. 2025;61:214–223.
3. Caravan P, Ellison JJ, McMurry TJ, et al. Gadolinium(III) chelates as MRI contrast agents: structure, dynamics, and applications. *Chem Rev*. 1999;99:2293–2352.
4. Forsting M, Palkowitsch P. Prevalence of acute adverse reactions to gadobutrol–a highly concentrated macrocyclic gadolinium chelate: review of 14,299 patients from observational trials. *Eur J Radiol*. 2010; 74:e186–e192.
5. Bruder O, Schneider S, Nothnagel D, et al. Acute adverse reactions to gadolinium-based contrast agents in CMR: multicenter experience with 17,767 patients from the EuroCMR Registry. JACC Cardiovasc Imaging2011;4:1171–1176.
6. Grobner T. Gadolinium—a specific trigger for the development of nephrogenic fibrosing dermopathy and nephrogenic systemic fibrosis? *Nephrol Dial Transplant*. 2006;21:1104–1108.
7. Marckmann P, Skov L, Rossen K, et al. Nephrogenic systemic fibrosis: suspected causative role of gadodiamide used for contrast-enhanced magnetic resonance imaging. *J Am Soc Nephrol*. 2006;17:2359–2362.
8. Mallepally A, Kidd JM, Grizzard JD, et al. Nephrogenic systemic fibrosis in patients with advanced renal dysfunction following gadolinium-based contrast agents. *Radiology*. 2025;317:e251794.
9. Kanda T, Ishii K, Kawaguchi H, et al. High signal intensity in the dentate nucleus and globus pallidus on unenhanced T1-weighted MR images: relationship with increasing cumulative dose of a gadolinium-based contrast material. *Radiology*. 2014;270:834–841.
10. Errante Y, Cirimele V, Mallio CA, et al. Progressive increase of T1 signal intensity of the dentate nucleus on unenhanced magnetic resonance images is associated with cumulative doses of intravenously administered gadodiamide in patients with normal renal function, suggesting dechelation. *Invest Radiol*. 2014;49:685–690.
11. McDonald RJ, McDonald JS, Kallmes DF, et al. Gadolinium deposition in human brain tissues after contrast-enhanced MR imaging in adult patients without intracranial abnormalities. *Radiology*. 2017;285:546–554.
12. Lohrke J, Frisk AL, Frenzel T, et al. Histology and gadolinium distribution in the rodent brain after the administration of cumulative high doses of linear and macrocyclic gadolinium-based contrast agents. *Invest Radiol*. 2017;52:324–333.
13. Radbruch A, Weberling LD, Kieslich PJ, et al. Gadolinium retention in the dentate nucleus and globus pallidus is dependent on the class of contrast agent. *Radiology*. 2015;275:783–791.
14. Quattrocchi CC, Mallio CA, Errante Y, et al. Gadodiamide and dentate nucleus T1 hyperintensity in patients with meningioma evaluated by multiple follow-up contrast-enhanced magnetic resonance examinations with no systemic interval therapy. *Invest Radiol*. 2015;50:470–472.
15. McDonald RJ, McDonald JS, Kallmes DF, et al. Intracranial gadolinium deposition after contrast-enhanced MR imaging. *Radiology*. 2015;275:772–782.
16. Kanda T, Fukusato T, Matsuda M, et al. Gadolinium-based contrast agent accumulates in the brain even in subjects without severe renal dysfunction: evaluation of autopsy brain specimens with inductively coupled plasma mass spectroscopy. *Radiology*. 2015;276:228–232.
17. Pietsch H, Lengsfeld P, Jost G, et al. Long-term retention of gadolinium in the skin of rodents following the administration of gadolinium-based contrast agents. *Eur Radiol*. 2009;19:1417–1424.
18. Idee JM, Port M, Robic C, et al. Role of thermodynamic and kinetic parameters in gadolinium chelate stability. *J Magn Reson Imaging*. 2009; 30:1249–1258.
19. Frenzel T, Lengsfeld P, Schirmer H, et al. Stability of gadolinium-based magnetic resonance imaging contrast agents in human serum at 37 degrees C. *Invest Radiol*. 2008;43:817–828.
20. Tweedle MF, Wedeking P, Kumar K. Biodistribution of radiolabeled, formulated gadopentetate, gadoteridol, gadoterate, and gadodiamide in mice and rats. *Invest Radiol*. 1995;30:372–380.
21. European Medicines Agency. EMA's final opinion confirms restrictions on use of linear gadolinium agents in body scans. 2017. Accessed September 5, 2026. https://www.ema.europa.eu/en/documents/press-release/emas-final-opinion-confirms-restrictions-use-linear-gadolinium-agents-body-scans_en.pdf.
22. Davies J, Siebenhandl-Wolff P, Tranquart F, et al. Gadolinium: pharmacokinetics and toxicity in humans and laboratory animals following contrast agent administration. *Arch Toxicol*. 2022;96:403–429.
23. Hall JE, Hall ME. Urine Concentration and dilution; regulation of extracellular fluid osmolarity and sodium concentration. *Guyton and Hall Textbook of Medical Physiology*, 14th edn. Philadelphia: Elsevier; 2020: 365–382.
24. Kümmerer K, Helmers E. Hospital effluents as a source of gadolinium in the aquatic environment. *Environ Sci Technol*. 2000;34:573–577.
25. Athmer M, Marotz L, Karst U. Rapid and sensitive speciation analysis of established and emerging gadolinium-based contrast agents in the aquatic environment by IC-ICP-MS. *J Anal At Spectrom*. 2025;40: 2138–2149.
26. Barrat JA, Bayon G, Tripier R, et al. Rare earth element abundances and gadolinium contamination in tap water worldwide. *Chemosphere*. 2025; 394:144812.
27. Le Fur M, Moon BF, Zhou IY, et al. Gadolinium-based Contrast Agent Biodistribution and Speciation in Rats. *Radiology*. 2023;309:e230984.
28. Davies J, Marino M, Smith APL, et al. Repeat and single dose administration of gadodiamide to rats to investigate concentration and location of gadolinium and the cell ultrastructure. *Sci Rep*. 2021;11: 13950.
29. Oh H, Chung YE, You JS, et al. Gadolinium retention in rat abdominal organs after administration of gadoxetic acid disodium compared to gadodiamide and gadobutrol. *Magn Reson Med*. 2020;84:2124–2132.
30. Bussi S, Coppo A, Celeste R, et al. Macrocyclic MR contrast agents: evaluation of multiple-organ gadolinium retention in healthy rats. *Insights Imaging*. 2020;11:11.
31. McDonald RJ, McDonald JS, Dai D, et al. Comparison of gadolinium concentrations within multiple rat organs after intravenous administration of linear versus macrocyclic gadolinium chelates. *Radiology*. 2017; 285:536–545.
32. Rasschaert M, Couloumy E, Renard E, et al. Overall gadolinium exposure within the first 5 months after injection of human equivalent doses of gadopiclenol, gadoterate, or gadobutrol in healthy rats. *Invest Radiol*. 2025;60:753–767.
33. Bücker P, Funke SKI, Factor C, et al. Combined speciation analysis and elemental bioimaging provide new insight into gadolinium retention in kidney. *Metallomics*. 2022;14:mfac004.
34. van der Molen AJ, Quattrocchi CC, Mallio CA, et al. Ten years of gadolinium retention and deposition: ESMRMB-GREC looks backward and forward. *Eur Radiol*. 2024;34:600–611.
35. Le Fur M, Caravan P. The biological fate of gadolinium-based MRI contrast agents: a call to action for bioinorganic chemists. *Metallomics*. 2019;11:240–254.
36. Strzeminska I, Factor C, Jimenez-Lamana J, et al. Comprehensive speciation analysis of residual gadolinium in deep cerebellar nuclei in rats repeatedly administered with gadoterate meglumine or gadodiamide. *Invest Radiol*. 2022;57:283–292.
37. Strzeminska I, Factor C, Robert P, et al. Speciation analysis of gadolinium in the water-insoluble rat brain fraction after administration of gadolinium-based contrast agents. *Invest Radiol*. 2021;56: 535–544.
38. Gianolio E, Bardini P, Arena F, et al. Gadolinium retention in the rat brain: assessment of the amounts of insoluble gadolinium-containing species and intact gadolinium complexes after repeated administration of gadolinium-based contrast agents. *Radiology*. 2017;285:839–849.
39. Frenzel T, Apte C, Jost G, et al. Quantification and assessment of the chemical form of residual gadolinium in the brain after repeated administration of gadolinium-based contrast agents: comparative study in rats. *Invest Radiol*. 2017;52:396–404.
40. Gianolio E, Gregorio ED, Aime S. Chemical insights into the issues of Gd retention in the brain and other tissues upon the administration of Gd-containing MRI contrast agents. *Eur J Inorganic Chem*. 2018;2019: 137–151.
41. US Food and Drug Administration. Guidance for Industry: Estimating the Maximum Safe Starting Dose in Initial Clinical Trials for Therapeutics in Adult Healthy Volunteers. White Oak, MD: US Food and Drug Administration; 2005.



*Copyright © 2026 The Author(s). Published by Wolters Kluwer Health, LLC.*

42. Hummel L, Frenzel T, Boyken J, et al. Comprehensive analysis of the spatial distribution of gadolinium, iron, manganese, and phosphorus in the brain of healthy rats after high-dose administrations of gadodiamide and gadobutrol. *Invest Radiol*. 2024;59:150–164.
43. Gladytz T, Millward JM, Cantow K, et al. Reliable kidney size determination by magnetic resonance imaging in pathophysiological settings. *Acta Physiol (Oxf)*. 2021;233:e13701.
44. Pohlmann A, Cantow K, Huelnhagen T, et al. Experimental MRI monitoring of renal blood volume fraction variations En route to renal magnetic resonance oximetry. *Tomography*. 2017;3:188–200.
45. Pohlmann A, Hentschel J, Fechner M, et al. High temporal resolution parametric MRI monitoring of the initial ischemia/reperfusion phase in experimental acute kidney injury. *PLoS One*. 2013;8:e57411.
46. Barry JA, Groseclose MR, Fraser DD, et alRevised preparation of a mimetic tissue model for quantitative imaging mass spectrometry. Protocol Exchange. 2018. doi:10.1038/protex.2018.104
47. Lohrke J, Berger M, Frenzel T, et al. Preclinical profile of gadoquatrane: a novel tetrameric, macrocyclic high relaxivity gadolinium-based contrast agent. *Invest Radiol*. 2022;57:629–638.
48. Kirchin MA, Pirovano GP, Spinazzi A. Gadobenate dimeglumine (Gd-BOPTA). An overview. *Invest Radiol*. 1998;33:798–809.
49. Jost G, Frenzel T, Boyken J, et al. Long-term excretion of gadolinium-based contrast agents: linear versus macrocyclic agents in an experimental rat model. *Radiology*. 2019;290:340–348.
50. van der Molen AJ, Dekkers IA, Geenen RWF, et al. Waiting times between examinations with intravascularly administered contrast media: a review of contrast media pharmacokinetics and updated ESUR Contrast Media Safety Committee guidelines. *Eur Radiol*. 2024;34:2512–2523.
51. Bücker P, Richter H, Radbruch A, et al. Deposition patterns of iatrogenic lanthanum and gadolinium in the human body depend on delivered chemical binding forms. *J Trace Elem Med Biol*. 2021;63:126665.
52. Herring N, Paterson DJ. *Blood vessel structure Levick's Introduction to Cardiovascular Physiology*, 6th edn. CRC Press (Taylor & Francis); 2018:9–10.
53. Rollhäuser H, Kriz W, Heinke W. Das Gefäss-System der Rattenniere [The Vascular System of the Rat Kidney]. *Zeitschrift für Zellforschung und Mikroskopische Anatomie*. 1964;64:381–403.
54. Kriz W. Der architektonische und funktionelle Aufbau der Rattenniere [The Architectural and Functional Structure of the Rat Kidney]. *Zeitschrift für Zellforschung und Mikroskopische Anatomie*. 1967;82:495–535.
55. Nordsletten DA, Blackett S, Bentley MD, et al. Structural morphology of renal vasculature. *Am J Physiol Heart Circ Physiol*. 2006;291:H296–H309.
56. Cantow K, Evans RG, Grosenick D, et al. Quantitative assessment of renal perfusion and oxygenation by invasive probes: basic concepts. *Methods Mol Biol*. 2021;2216:89–107.
57. Harpur ES, Worah D, Hals PA, et al. Preclinical safety assessment and pharmacokinetics of gadodiamide injection, a new magnetic resonance imaging contrast agent. *Invest Radiol*. 1993;28(suppl 1):S28–S43.
58. Steger-Hartmann T, Graham PB, Muller S, et al. Preclinical safety assessment of Vasovist (Gadofosveset trisodium), a new magnetic resonance imaging contrast agent for angiography. *Invest Radiol*. 2006;41:449–459.
59. Döhr O, Hofmeister R, Treher M, et al. Preclinical safety evaluation of Gd-EOB-DTPA (Primovist). *Invest Radiol*. 2007;42:830–841.
60. Wack C, Steger-Hartmann T, Mylecraine L, et al. Toxicological safety evaluation of gadobutrol. *Invest Radiol*. 2012;47:611–623.
61. Dobrota M, Powell CJ, Holtz E, et al. Biochemical and morphological effects of contrast media on the kidney. *Acta Radiol Suppl*. 1995;399:196–203.
62. Morcos SK, Epstein FH, Haylor J, et al. Aspects of contrast media nephrotoxicity. *Eur J Radiol*. 1996;23:178–184.
63. Han MW, Kim PH, Suh CH, et al. Risk of acute kidney injury following gadolinium-based contrast agent-enhanced MRI: propensity-matched 7-year cohort study. *Invest Radiol*. 2026;61:334–340.
64. Hall JE, Hall ME. *The Urinary System: Functional Anatomy and Urine Formation by the Kidneys Guyton and Hall Textbook of Medical Physiology*, 14th edn. Philadelphia: Elsevier; 2020:321–330.
65. Maimouni I, Henoumont C, De Goltstein MC, et al. Gadopiclenol: a q = 2 gadolinium-based MRI contrast agent combining high stability and efficacy. *Invest Radiol*. 2025;60:234–243.


*Copyright © 2026 The Author(s). Published by Wolters Kluwer Health, LLC.*